

Finite Element Modeling of 3D Orthogonal Woven C/C Composite Based on Micro-Computed Tomography Experiment

Ai Shigang · Zhu Xiaolei · Mao Yiqi · Pei Yongmao · Fang Daining

Received: 21 August 2013 / Accepted: 1 October 2013 / Published online: 22 October 2013
© Springer Science+Business Media Dordrecht 2013

Abstract Two-dimensional images of C/C 3D orthogonal woven composite were captured by X-ray micro-computed tomography (μ CT). The μ CT data reveal comprehensive mesogeometrical information about the carbon fiber tows, carbon matrix, and void defects etc. The fibers tows are characterized consisting of the cancroids of a tow, the area and aspect ratio of its cross-section. A statistical analysis of the volume fraction and positioning of the void defects in the 3D orthogonal woven architecture is performed based on 2-D micro tomography images. The tabulated statistics are sufficient to generate the virtual specimen, which shares the same statistical characteristics of the C/C composite and the void defects are included. Three-point bending experiment and simulation are carried out and the results show that the finite element model including the void defects gives more accurate results. The finite element model will give some highlights to the numerical simulation approach of the C/C textile composite under thermal, mechanical and oxygen coupled service environment. And the numerical techniques for modelling such kind materials with woven architecture and void defects are recommended.

Keywords Finite element modelling · C/C composite · 3D orthogonal woven · Matrix void defects · Micro-computed tomography

1 Introduction

3D woven composites are increasingly important material options for many types of structures such as aircraft, ships, armour protection and so on [1–5]. The fibre architecture of 3D orthogonal woven composites consists of in-plane layers of warp (0°) and weft (90°) fibrous yarns interlocked with z-binder yarns in the through-thickness direction. Researches have shown that the z-binders improved the delamination toughness, impact damage resistance, and post-impact mechanical properties of the 3D orthogonal woven composites [6, 7]. For high performance and reliability of the 3D orthogonal textile reinforcement, a key

A. Shigang · Z. Xiaolei · M. Yiqi · P. Yongmao · F. Daining (✉)
State Key Laboratory of Tubulence and Complex System, College of Engineering,
Peking University, Beijing, China 100871
e-mail: sgai@pku.edu.cn

issue is the internal defects, such as micro-cracks, voids and so on. The defects can be substantial perturbations of the ideal architecture of the materials which trigger the failure mechanisms and compromise strength. For applications in pivotal fields such as the aerospace industry, it is desired to arise on the capability to predict the influence of defects on performance of the materials. And for the first step, it is to characterize the type and statistical distribution of the defects and reconstruct the virtual specimens of the materials for numerical analysis, which has proven extremely difficult using conventional imaging techniques.

In the last several decades, a number of methods for generating solid models of textile reinforcement have been presented. In Lomov et al's work [8, 9], an orderly approach to construct FE model of textile composites was presented, based on the geometrical modeller WiseTex, commercial ANSYS and custom-developed SACOM FE packages. In Hivet and Boisse's work [10, 11], geometrical model of 2D fabrics was constructed and experimental observations had been performed to determine real yarn geometry in different cases of yarn structure and weaving using different optical processes. In references [12–20], different types of meso-structure models of textile composites were presented, and the mechanical properties of the composites were numerically analyzed. In those studies, tow surfaces were assumed consisting of a combination of flat segments where two tows contact one another, but without analyzing tow shapes with experimental specimens. In recent years, X-ray micro-computed tomography (μ CT) technology has been used and proved as an effective approach to characterize the micro-structure of textile composites. In Cox et al's work [21–25], three-dimensional images of textile composites were captured by X-ray μ CT on a synchrotron beamline. Based on a modified Markov Chain algorithm and the μ CT data, a computationally efficient method has been demonstrated for generating virtual textile specimens. In Desplentere et al's work [26], X-ray μ CT was used to characterize the micro-structural variation of four different 3D warp-interlaced fabrics. Based on the μ CT data, virtual specimens of four types of 3D warp-interlaced fabrics reconstructed and the in-plane mechanical properties of the four kinds of materials were studied. And the influence of the variability of the fabric internal geometry on the mechanical properties of the composites was estimated. In those studies, meso-structures of fiber tows were reconstructed and which share the statistical characteristics of the specimens analyzed by the μ CT. However, generally speaking, the reconstruction of the virtual specimen is really a huge and complex work, sometimes, the virtual specimens explored through this approach are difficult to use for numerical analysis for the excessive geometry information.

In this article, the composite investigated is C/C 3D orthogonal woven composite for high-temperature applications, where both strength and high-temperature oxidation are important. Defects, such as matrix voids and micro-cracks, have significant influences on the failure factors and high-temperature oxidation behaviours of the C/C materials and structures in thermal-mechanical-oxygen coupled serves environment. So, it is desired to explore the FE model of the C/C 3D orthogonal woven composite for numerical analysis. The FE model should be reasonably simple for thermal-mechanical-oxygen coupled analysis, at the same time, the geometry information of the voids and micro-cracks should be included.

In this work, firstly, the meso-structure of the C/C composite is investigated by μ CT with the spatial resolution of 50 μ m and the 2-D images of the specimens at different sections are generated. For reconstruction of tow architecture, the section shapes and the space trajectory of the fiber tows are statistically analyzed and the geometrical models of the 3D orthogonal woven yarns are constructed. In the meso-structure model, the sections of the warp tows and weft tows are assumed as oval and the section of the z-binder yarns is assumed as circular.

The radius of the z-binder yarns, the long-axis and the short-axis of the warp and weft tows are yield from the μ CT experiments. Secondly, the geometrical model of the carbon matrix is generated by Boolean operation. A key challenge is to develop probabilistic methods of predicting the volume fraction and distribution of the matrix voids using the μ CT data. For that, a C++ procedure is explored to statistically analyze the volume and distribution of the matrix voids by a binary analysis approach. The volume fraction of the voids located at the fiber/matrix interface is studied carefully. Then the FE model of the C/C composite with the matrix void defects is constructed, static tensile and three-point bending simulations are carried out and discussed.

2 Computational Procedure

2.1 Subject Material

Material studied in this article is C/C 3-D orthogonal woven ceramic composite in which T300 carbon fiber (Nippon Toray, Japan) tows rigidified by carbon matrix, as shown in Fig. 1a. The spatial configuration of the 3-D orthogonal fiber preforms and the composite (fabricated by National Key Laboratory of Thermostructure Composite Materials, Northwestern Polytechnical University, China) are illustrated in Fig. 1b. The C/C composites were prepared using chemical vapor infiltration (CVI) method. Firstly, T300 carbon fiber was employed to prepare the 3-D orthogonal fiber preforms which were used as reinforcement of the C/C composites. The fiber volume fraction in the preforms was controlled at about 56.5 %. Secondly, pyrolytic carbon was deposited on the surface of the preforms though CVI approach in order to modify the C_{fiber}/C_{matrix} interface. Then the preforms were infiltrated with carbon by CVI, depositing some material on individual fibers in the interior regions of each tow before sealing the tow perimeter. Finally, the fiber preforms were infiltrated with carbon matrix using multiple cycles of infiltration and heat treatment at 1373 K, 0.03 MPa. With increasing cycles, a matrix with near full density can be asymptotically approached; generally, it was about 10 cycles (1200 h).

Fiber tows in the 3-D orthogonal woven process are approximately elliptical cross-sections. The tows fit together snugly in the woven pattern by a system of periodic motions, and approximately in the same cross-sectional area and aspect ratio. In this study, the shapes of the tow cross-sections of the warp fiber and weft fiber are fitted as ellipse and the area and the ellipse aspect ratio are recorded. The cross-sections of the z-binder tows are fitted as circular. Attention is restricted to generate replicas of the carbon fiber tows and the carbon matrix in which voids are located randomly. The matrix void defects are illustrated in Fig. 1c.

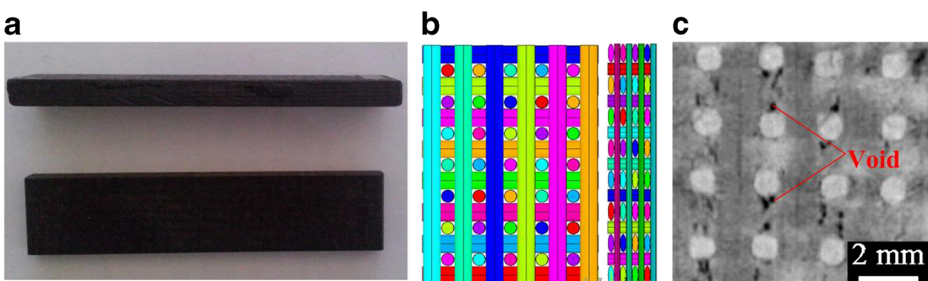


Fig. 1 a C/C 3-D orthogonal woven composite, b 3-D orthogonal woven architecture, c void defects

2.2 Measurement of Fiber tow Cross-Sections

The first step in Meso-FE modeling of the C/C woven composite is to identify the cross-section shapes of the warp tows, weft tows and the z-binder tows based on X-ray μ CT experiments. The X-ray μ CT images were acquired with the SanYing nanoVoxel-2000 microfocus X-ray system. The scans were conducted with X-rays at a voltage of 30 kV and a current of 0.5 mA. The images have a pixel size of 50 μ m and the specimens for the CT measurements is cut by the size of 10 mm \times 10 mm \times 5 mm. Sixty four frames were acquired by rotating the samples with increments of 0.25°. The 3D data was stored in 500 cross-sectional slices, each slice providing a cross-section of the material with dimensions 5 mm \times 10 mm or 10 mm \times 10 mm, depending on the directions. A big advantage of this measuring method is the fact that the positions of the cross-sections are well known. Each pixel in the data slices is 50 μ m on a side, and each slice is separated by one pixel. To measure the different dimensions and spacing of the yarns, a data analysis procedure described following in Section 2.3 was applied to the μ CT images, as shown in Fig. 2. For each parameter, at least 50 measurements were performed. These 50 measurements were distributed over several samples taken all over the embedded fabric. In this way, a good characterization of the variation of the composite meso-structure is obtained.

As illustrated in Fig. 2a, the diameter of the z-binder fiber tows is ' d ', and the space between tow z-binder tows is ' l '. By at least 50 measurements, the ratio of $l:d$ is 1:0.425 and $d=0.85$ mm. For the warp fiber tows and the weft fiber tows, the cross-sections are fitted as ellipse. The long axis and the short axis of the ellipse is ' a ' and ' b ' correspondingly, as shown in Fig. 2b. By at least 50 measurements, $a:b=1:0.326$ and $a=1.15$ mm, $b=0.37$ mm.

2.3 Measurement of Void Defects

In the X-ray μ CT scanning process, the external environment, devices and images transition in conversion process all will make the μ CT images blurredly. Therefore, to extract useful information from the μ CT images, it must be have a pre-enhance process to improve the contrast of those photos. In this study, a MATLAB procedure is used to deal with the μ CT

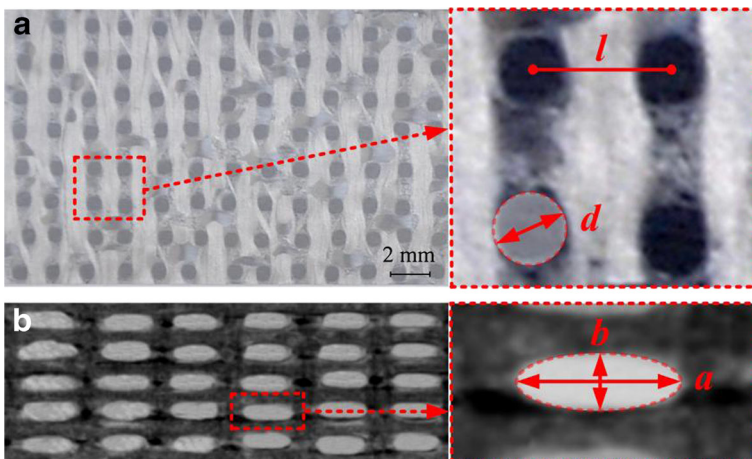


Fig. 2 Cross-sections of the carbon fiber tows, **a** z-binder tows, **b** warp tows and weft tows

images of the 3-D orthogonal woven C/C material cross-sectional slices to reduce noises and enhance the effective information. The pre-enhance process is diagramed in Fig. 3.

There exists obvious difference between the carbon matrix and voids in the gray-scale, and therefore, a gray threshold is used to separate voids from the images in binarization processing. Then the determining of the threshold is very important in the present problem. There are several methods to determine the threshold, such as histogram troughs law, OTSU segmentation method, maximum entropy method and so on. In this study, the maximum entropy is adopted.

Maximum entropy method firstly proposed by Pun [27]. This approach is used to divide the gray-level histogram of images into separate classes and make maximum total entropy of all kinds of classes. “S” is a potential segmentation threshold point, $p_0, p_1, p_2, \dots, p_L$ is the probability distribution of gray levels, then it is divided into two probability distributions

$$A : \frac{p_0}{p_d}, \frac{p_1}{p_d}, \frac{p_2}{p_d}, \dots, \frac{p_S}{p_d} \tag{1}$$

$$B : \frac{p_{S+1}}{1-p_d}, \frac{p_{S+2}}{1-p_d}, \frac{p_{S+3}}{1-p_d}, \dots, \frac{p_L}{1-p_d} \tag{2}$$

where, $p_d = \sum_{i=0}^S p_i$, L is the number of gray levels. Then, the entropy after segmentation image is calculated by the Eqs. 3–5.

$$H(S) = E_A + E_B \tag{3}$$

$$E_A = -\sum_{i=0}^S \frac{p_i}{p_d} \log\left(\frac{p_i}{p_d}\right) \tag{4}$$

$$E_B = -\sum_{i=S+1}^L \frac{p_i}{1-p_d} \log\left(\frac{p_i}{1-p_d}\right) \tag{5}$$

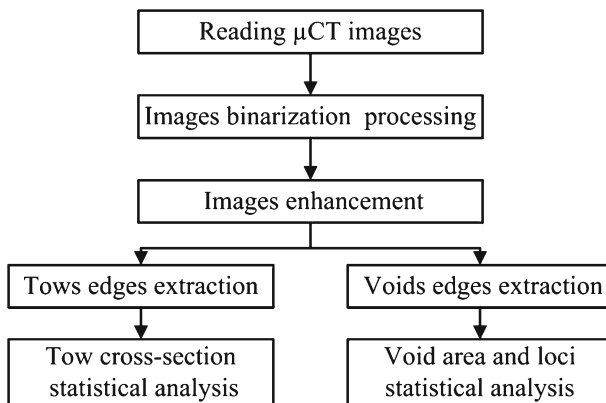


Fig. 3 Process of void defects statistically analyzes

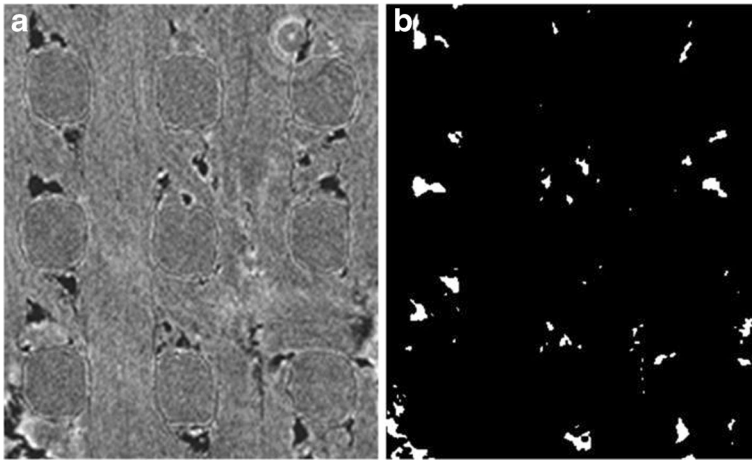


Fig. 4 Voids boundary extraction, **a** μCT image, **b** void defects

The best threshold value of image segmentation is shown in Eq. 6

$$H_o = \arg \max_S (H(S)) \tag{6}$$

If the exponential entropy is adopted, the entropy after segmentation image can be seen in Eq. 7 from the Eqs. 3–5,

$$H_N(S) = \sum_{i=0}^S \frac{p_i}{p_d} e^{1-\frac{p_i}{p_d}} + \sum_{i=S+1}^L \frac{p_i}{1-p_d} e^{1-\frac{p_i}{1-p_d}} \tag{7}$$

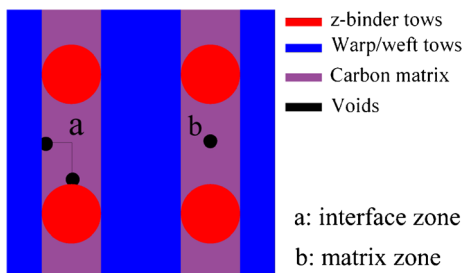
Then, the optimal threshold value of divided images is shown in Eq. 8,

$$H_o = \arg \max_S (H_N(S)) \tag{8}$$

Image enhancement is an operation to remove noises and highlight useful information. For the μCT images, the noise is mainly caused by the basic properties of light and electricity, and this noise may be enhanced to “salt & pepper” noise after image binarization process. For this type of noise, the median filtering algorithm is very effective and hence adopted.

Extracting the external contour of the voids is an important step to statistical analysis of the void defects. The image edge detection is usually done by the first order or second order derivative. The common edge detection operator in MATLAB is Robert gradient operator, Sobel operator, Prewitt operator, Laplacian and so on. In this study, the “edge” function, which

Fig. 5 Diagram of the locations of void defects



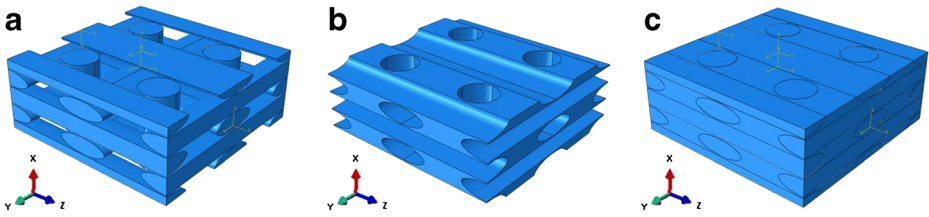


Fig. 6 Geometrical model of 3-D orthogonal textile C/C material, **a** carbon fiber tows, **b** carbon matrix, **c** whole composite

provided by the MATLAB, is adopted to detect the boundaries of voids by constructing Prewitt operator. The result is shown in Fig. 4. The area of the cross-sectional slice (Fig. 4a) is $2.99\text{ mm} \times 3.64\text{ mm} = 10.88\text{ mm}^2$ and there have 74 voids (Fig. 4b) with the total area of those voids is 0.29 mm^2 . For the 2-D image, the area fraction of the void defects is 2.67 %. For 3-D geometrical model, the volume fraction of the voids is calculated by the Eq. 9,

$$V_{void} = \left(\frac{A_{void}}{A} \right)^{3/2} \tag{9}$$

where, A_{void} is the total area of the voids in the 2-D image and ‘ A ’ is the area of the image. So, the voids volume fraction of the 3-D geometrical model is 0.44 %.

From the 2-D CT images, it is found that void defects almost all located in the C_{fiber}/C_{matrix} interface zone and the carbon matrix zone (situation ‘a’ and ‘b’ correspondingly, as shown schematically in Fig. 5), while the fiber tows are almost intact. It is also found that the numbers and areas of the voids in those two zones are different and more voids located in the C_{fiber}/C_{matrix} interface zone. So, in order to reveal the void defects more precisely in the virtual specimens, the areas of the voids in those two zones are statistically studied and $A_{interface}:A_{matrix} = 1.974:1$, then, $V_{interface}:V_{matrix} = 2.773:1$. The volume densities of the voids in those two zones are 0.32 % and 0.12 % correspondingly.

2.4 Generation of FE Model

As discussed in Section 2.2, the cross-section of the z-binder tows is fitted as circular and the radius is 0.85 mm. The cross-section of the warp tows and weft tows is fitted as ellipse with the ellipse aspect ratio is 1:0.326 and the long axis of the ellipse is 1.15 mm. A sub-procedure was explored to generate the geometrical model of the 3-D orthogonal textile

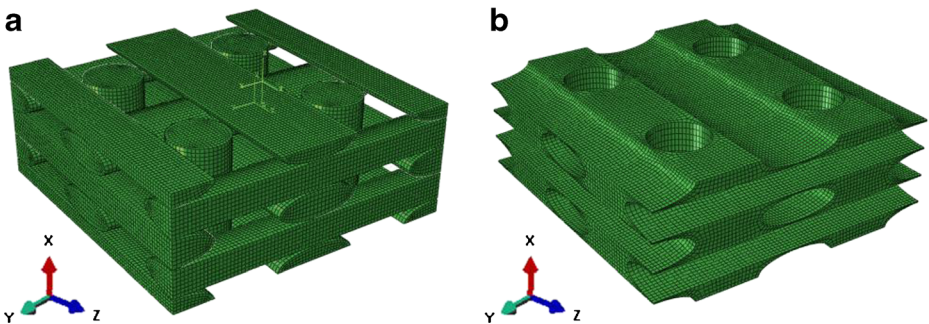


Fig. 7 Finite element mesh, **a** carbon fiber tows, **b** carbon matrix

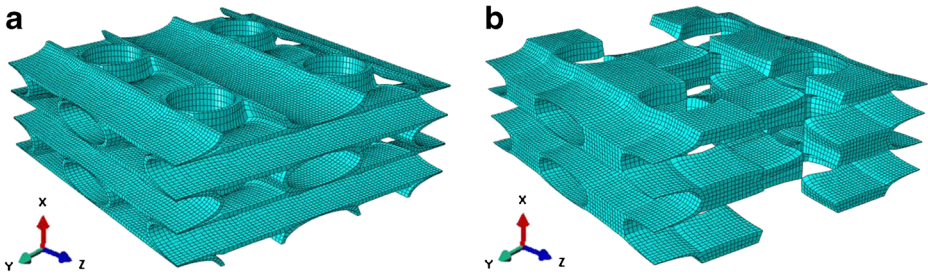


Fig. 8 Finite element set, **a** interface-set, **b** matrix-set

architecture of the *C/C* material based on Python code. First of all, the geometrical model of the carbon fiber tows is constructed, as shown in Fig. 6a. For carbon fiber, it is an orthogonality material, so, three local coordinates are constructed to identify the material directions of the warp, weft and z-binder tows respectively. Then, a rectangle solid model with the same size of the composite specimen is constructed and Boolean operation between the rectangle solid model and the fiber yarns' model carried out to generate the geometrical model of the carbon matrix, which is shown in Fig. 6b. A whole $2 \times 2 \times 2$ cell model of the composite are illustrated in Fig. 6c.

Generally, accuracy of FE simulations is significantly influenced by the quality of the finite element mesh. In this study, the warp, weft and z-binder tows are meshed by sweep meshing method and the element type is C3D8R, a hexahedral element with eight nodes, as shown in Fig. 7a. For the carbon matrix, as illustrated in Fig. 6b, the geometry is very complex. To mesh the geometry model of the matrix with high quality hexahedral elements, a FE mesh algorithm based on ABAQUS is explored and the matrix is meshed successfully with the element C3D8R, as shown in Fig. 7b. There are 124584 and 70912 elements for the carbon fiber tows and the carbon matrix correspondingly.

As discussed in Section 2.3, the volume densities of void defects in the C_{fiber}/C_{matrix} interface zone and the carbon matrix zone are different. So, to import void defects in those two regions respectively, the carbon matrix is divided into two sets, the interface-set and matrix-set. The interface-set (as shown in Fig. 8a) includes a single layer of elements attached around the fiber tows, while the matrix-set (as shown in Fig. 8b) includes all the matrix elements except the ones attached with the fiber tows. A Monte Carlo algorithm is presented to generate the void defects in the two sets. Elements are chosen one-by-one randomly as 'void defects' until the total volume of the 'void defects' reach the defect volume fraction. For the *C/C* composite studied in this paper, the volume densities of void

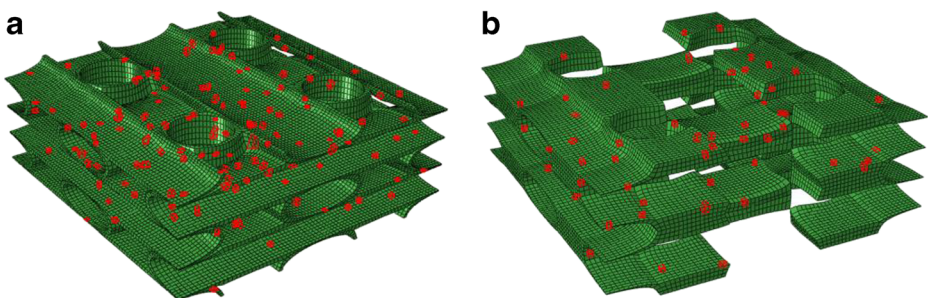


Fig. 9 Void defects, **a** interface zone, **b** matrix zone

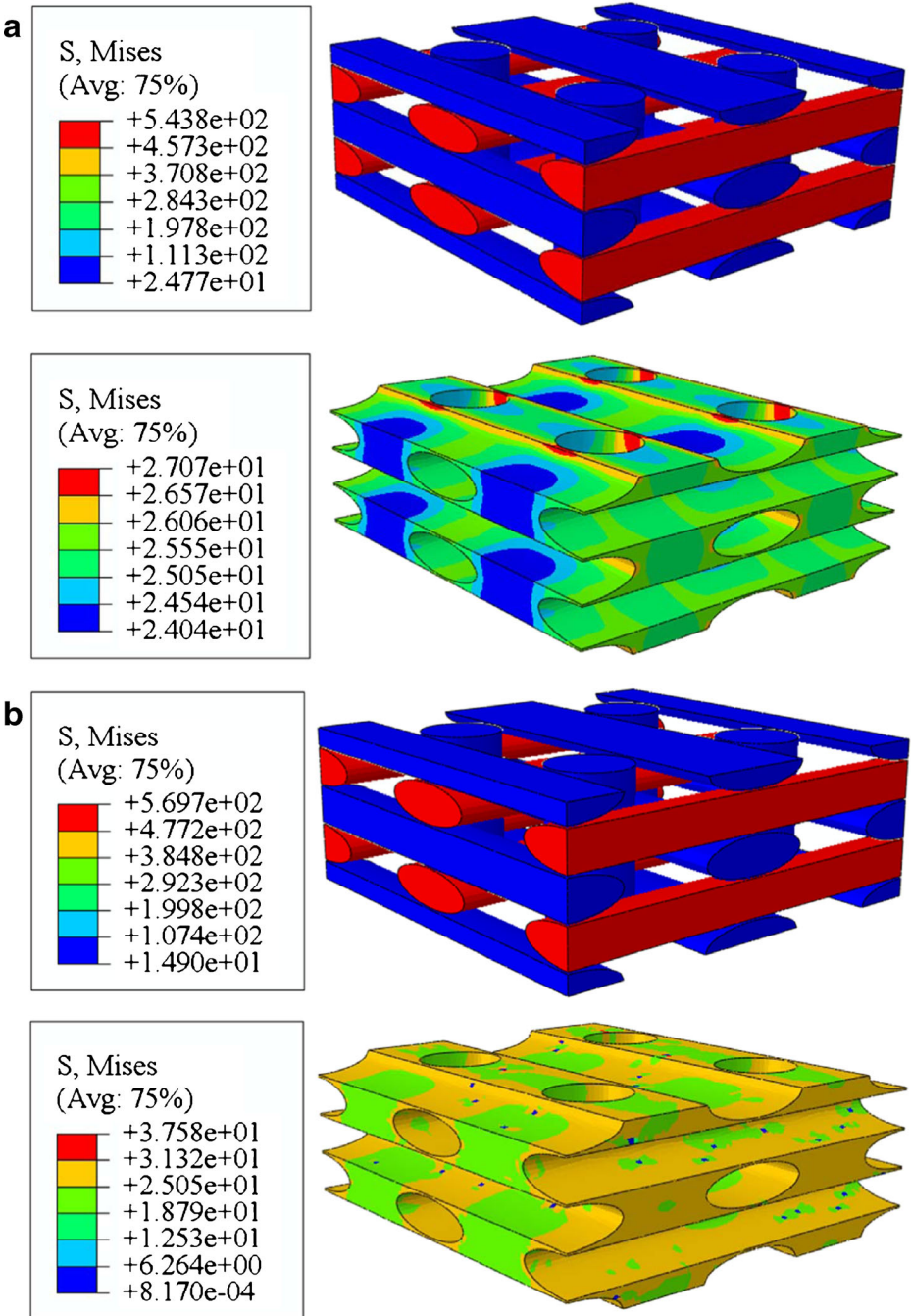


Fig. 10 Mises stress contour in static uniaxial tensile simulations, **a** intact model, **b** model with void defects

defects in the C_{fiber}/C_{matrix} interface zone and the matrix zone are 0.32 % and 0.12 % respectively. It must be noted out that those elements which identified as void defects are not

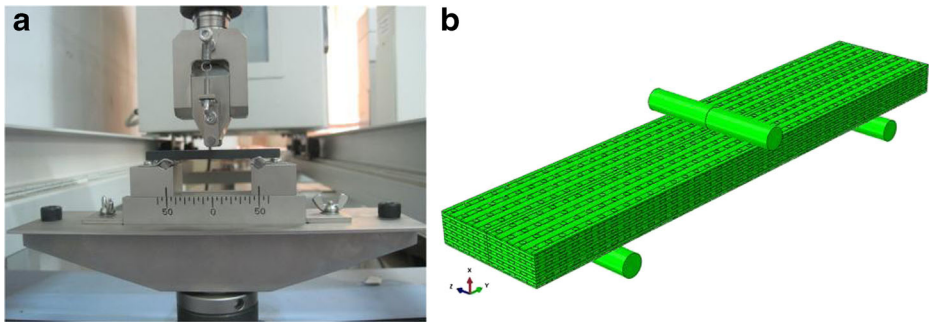


Fig. 11 Three-point bending test, **a** experiment, **b** FE modelling

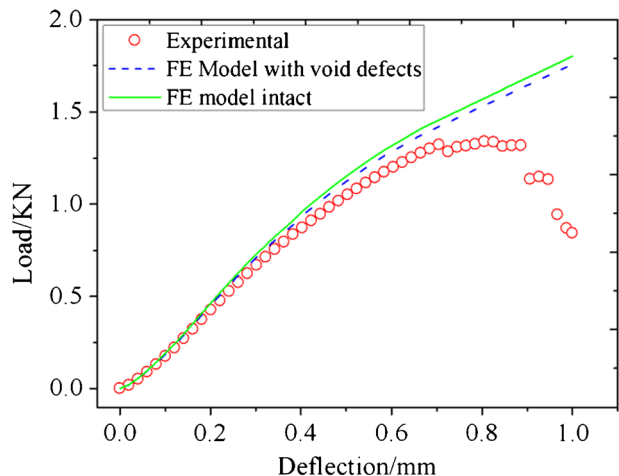
moved away from the FE model, but the stiffness of those elements are reduced by $10e-6$ times in simulations. The void defects in the C_{fiber}/C_{matrix} interface zone (130 elements in total) and the carbon matrix inner zone (53 elements in total) are shown in Fig. 9.

3 Finite Element Simulation

Static uniaxial tensile simulations are carried out based on Abaqus/standard code. In order to keep forces continuity and displacements compatibility of the opposite faces of the unit cell, periodic boundary conditions are imposed in the simulation. Because the opposite faces of the unit cell have the same geometrical features, the nodes on the faces are controlled in the same position to form the corresponding nodes in the process of FE meshing. The periodic BCs are imposed on the corresponding nodes by FORTRAN pre-compiler code, detailed in Ref. [28]. A constant displacement load is subjected to the top surface and the loading strain is 0.3 %.

Mises stress contour of the C/C composite specimens are illustrated in Fig. 10. For the carbon fiber tows, Mises stress contour have about 4.8 % difference between the defected model and the perfect model with the peak stress are 543.8 MPa and 569.7 MPa respectively. But for the carbon matrix, Mises stress contour have larger difference between the defected model and the perfect. For the model with void defects, the peak stress is about 37.6 MPa,

Fig. 12 Load-deflection curves in three-point bending experiment and numerical simulations



while for the perfect model, the peak value of Mises stress is about 27.1 MPa, with 38.7 % difference. The equivalent elastic tensile modulus calculated from the perfect model and the defected model is 46.8GPa and 46.6GPa respectively. From Fig. 10, for the defected specimen there have serious stress concentration besides the matrix voids and those locations probably where micro-cracks generated firstly.

To provide experimental benchmark for calibration of the proposed numerical model, a three-point bending simulation was carried out and the numerical results are compared with experimental results. The experiment equipments (Shimadzu WDW-10) and the C/C specimen are illustrated in Fig. 11a. In the three-point bending test, a constant displacement loading is adopted and the loading speed is 1 mm/min. The FE model for the three-point bending test is shown in Fig. 11b. Two specimens are constructed with one has matrix void defects and the other one is intact. The numerical results and the experimental result are illustrated in Fig. 12 and the numerical result from the FE model with void defects agreed well with the experimental result.

4 Conclusion

Meso-structure of C/C composite investigated by μ CT experiments, and the section shapes and the space trajectory of the fiber tows are statistically analyzed. Then the geometrical models of the 3D orthogonal woven composite are then constructed. A special focus is the void defects of the composite and which are statistically investigated based on the μ CT images. Therefore, a probabilistic method of predicting the volume fraction and distribution of the matrix voids is explored by a binary analysis approach. Especially, the volume densities of the voids located at the fiber/matrix interface zone and the matrix zone are investigated carefully. Then the FE model of the C/C composite is constructed with void defects included, and the static tensile and three-point bending properties are numerically analyzed. Comparing the numerical results with the experimental result, the FE model with void defects agree well with the experiment result. The FE model presented herein forms the first step in numerical analysis of the mechanical properties and failure behaviors of the C/C material under the thermal, mechanical and oxygen coupled loadings which the C/C material and structures suffered in service.

Acknowledgments Financial support from the National Natural Science Foundations of China (No. 11202007, 11232001) and the National Basic Research Program (973) of China (No. 2011CB606105) are gratefully acknowledged.

References

1. Miravete, A., Bielsa, J.M., Chiminelli, A., Cuartero, J., Serrano, S., Tolosana, N., Guzman, R.V.: 3D mesomechanical analysis of three-axial braided composite materials. *Compos. Sci. Technol.* **66**, 2954–2964 (2006)
2. Li, J.C., Chen, L., Zhang, Y.F., Pan, N.: Microstructure and finite element analysis of 3D five-directional braided composites. *J. Reinf. Plast. Comp.* **31**(2), 107–115 (2011)
3. Potluri, P., Hogg, P., Arshad, M., Jetavat, D., Jamshidi, P.: Influence of fibre architecture on impact damage tolerance in 3D woven composites. *Appl. Compos. Mater.* **19**(5), 799–812 (2012)
4. Zhang, R.B., Chen, G.Q., Han, W.B.: Synthesis, mechanical and physical properties of bulk Zr₂Al₄C₅ ceramic. *Mater. Chem. Phys.* **119**(1–2), 261–265 (2010)

5. Ma, J.Q., Xu, Y.D., Zhang, L.T., Cheng, L.F., Nie, J.J., Dong, N.: Microstructure characterization and tensile behavior of 2.5D C/SIC composites fabricated by chemical vapor infiltration. *Scripta. Mater* **54**, 1967–1971 (2006)
6. Bejan, L., Taranu, N., Sirbu, A.: Effect of hybridization on stiffness properties of woven textile composites. *Appl. Compos. Mater.* **20**(2), 185–194 (2013)
7. Yao, L., Wang, X., Xu, F.J., Jiang, M.W., Zhou, D.C., Qiu, Y.P.: Effect of wire space and weaving pattern on performance of microstrip antennas integrated in the three dimensional orthogonal woven composites. *Appl. Compos. Mater.* **19**(1), 21–30 (2012)
8. Lomov, S.V., Ivanov, D.S., Verpoest, I., Zako, M., Kurashiki, T., Nakai, H., Hirotsawa, S.: Meso-FE modelling of textile composites: road map, data flow and algorithms. *Compos. Sci. Technol.* **67**, 1870–1891 (2007)
9. Lomov, S.V., Perie, G., Ivanov, D.S., Verpoest, I., Marsal, D.: Modeling three-dimensional fabrics and three-dimensional reinforced composites: challenges and solutions. *Text. Res. J.* **81**(1), 28–41 (2011)
10. Hivet, G., Boisse, P.: Consistent 3D geometrical model of fabric elementary cell. Application to a meshing preprocessor for 3D finite element analysis. *Finite Elem. Anal. Des.* **42**, 25–49 (2005)
11. Hivet, G., Boisse, P.: Consistent mesoscopic mechanical behaviour model for woven composite reinforcements in biaxial tension. *Compos. Part B* **39**, 345–361 (2008)
12. Miao, Y.Y., Zhou, E., Wang, Y.Q., Cheeseman, B.A.: Mechanics of textile composites: micro-geometry. *Compos. Sci. Technol.* **68**, 1671–1678 (2008)
13. Wang, Y.Q., Sun, X.K.: Digital-element simulation of textile processes. *Compos. Sci. Technol.* **61**, 311–319 (2001)
14. Cuong, H.M., Boussu, F., Kanit, T., Crepin, D., Imad, A.: Effect of frictions on the ballistic performance of a 3D warp interlock fabric: numerical analysis. *Appl. Compos. Mater.* **19**(3–4), 333–347 (2012)
15. Hage, C.E., Younès, R., Aboura, Z., Benzeggagh, M.L., Zoaeter, M.: Analytical and numerical modeling of mechanical properties of orthogonal 3D CFRP. *Compos. Sci. Technol.* **69**, 111–116 (2009)
16. Feng, M.L., Wu, C.C.: A study of three-dimensional four-step braided piezo-ceramic composites by the homogenization method. *Compos. Sci. Technol.* **61**, 1889–1898 (2001)
17. Tolosana, N., Carrera, M., Villoria, R.G., Castejon, L., Miravete, A.: Numerical analysis of three-dimensional braided composite by means of geometrical modeling based on machine emulation. *Mech. Adv. Mater. Struc.* **19**, 207–215 (2012)
18. Mao, J.Z., Sun, X.S., Ridha, M., Tan, V.B.C., Tay, T.E.: A modeling approach across length scales for progressive failure analysis of woven composites. *Appl. Compos. Mater.* **20**(3), 213–231 (2013)
19. Xiao, X.R., Kia, H.G., Gong, X.J.: Strength prediction of a triaxially braided composite. *Compos. Part A* **42**, 1000–1006 (2011)
20. Ullah, H., Harland, A.R., Silberschmidt, W.: Experimental and numerical analysis of damage in woven GFRP composites under large-deflection bending. *Appl. Compos. Mater.* **19**(5), 769–783 (2012)
21. Bale, H., Blacklock, M., Begley, M.R., Marshall, D.B., Cox, B.N., Ritchie, R.O.: Characterizing three-dimensional textile ceramic composites using synchrotron X-Ray micro-computed-tomography. *J. Am. Ceram. Soc.* **95**(1), 392–402 (2012)
22. Rinaldi, R.G., Blacklock, M., Bale, H., Begley, M.R., Cox, B.N.: Generating virtual textile composite specimens using statistical data from micro-computed tomography: 3D tow representations. *J. Mech. Phys. Solids.* **60**, 1561–1581 (2012)
23. Blacklock, M., Bale, H., Begley, M., Begley, M.R., Cox, B.N.: Generating virtual textile composite specimens using statistical data from micro-computed tomography: 1D tow representations for the Binary Model. *J. Mech. Phys. Solids.* **60**, 451–470 (2012)
24. Yang, Q.D., Cox, B.N.: Predicting failure in textile composites using the Binary Model with gauge-averaging. *Eng. Fract. Mech.* **77**, 3174–3189 (2010)
25. Vanaerschot, A., Cox, B.N., Lomov, S.V., Vandepitte, D.: Stochastic framework for quantifying the geometrical variability of laminated textile composites using micro-computed tomography. *Compos. Part A* **44**, 122–131 (2013)
26. Desplentere, F., Lomov, S.V., Woerdeman, D.L., Verpoest, I., Wevers, M., Bogdanovich, A.: Micro-CT characterization of variability in 3D textile architecture. *Compos. Sci. Technol.* **65**, 1920–1930 (2005)
27. Pun, T.: A new method for gray-level picture thresholding using the entropy of the histogram. *Signal Process.* **2**, 223–237 (1980)
28. Ai, S.G., Mao, Y.Q., Pei, Y.M., Fang, D.N., Tang, L.Q.: Effect of stitching angle on mechanical properties of stitched sandwich panels. *Mater. Design.* **50**, 817–824 (2013)